Imaging of CO_2 Injection during an Enhanced-Oil-Recovery Experiment

Roland Gritto[1], Thomas M. Daley[1], and Larry R. Myer[1]
[1]Lawrence Berkeley National Laboratory
One Cyclotron Road, MS 90-1116
Berkeley CA, 94720, USA

Abstract

A series of time-lapse seismic cross well and single well experiments were conducted in a diatomite reservoir to monitor the injection of CO_2 into a hydrofracture zone, using P- and S-wave data. During the first phase the set of seismic experiments were conducted after the injection of water into the hydrofrac-zone. The set of seismic experiments was repeated after a time period of 7 months during which CO_2 was injected into the hydrofractured zone. The issues to be addressed ranged from the detectability of the geologic structure in the diatomic reservoir to the detectability of CO_2 within the hydrofracture.

During the pre-injection experiment, the P-wave velocities exhibited relatively low values between 1700-1900 m/s, which decreased to 1600-1800 m/s during the post-injection phase (-5%). The analysis of the pre-injection S-wave data revealed slow S-wave velocities between 600-800 m/s, while the post-injection data revealed velocities between 500-700 m/s (-6%). These velocity estimates produced high Poisson ratios between 0.36 and 0.46 for this highly porous (~ 50%) material. Differencing post- and pre-injection data revealed an increase in Poisson ratio of up to 5%. Both, velocity and Poisson estimates indicate the dissolution of CO_2 in the liquid phase of the reservoir accompanied by a pore-pressure increase. The results of the cross well experiments were corroborated by single well data and laboratory measurements on core data.

Introduction

A subsurface CO_2 injection program was operated by Chevron USA Production Company in the Lost Hills, California, oil field (Figure 1). This pilot program, which is partially funded by the U.S. Department of Energy (DOE) as an enhanced oil recovery (EOR) project, was ideally suited for design and testing of geologic CO_2 sequestration concepts including subsurface monitoring techniques.

The success of CO_2 sequestration will depend greatly on the reservoir properties. The diatomite reservoirs of central California have unusually high porosity (45-70%) and low permeability (< 1 millidarcy). The pore size is < 5 microns while the pore space is occupied by a mixture of water (50%), oil (45%), and gas (5%) (Perri et al., 2000). Because of the low permeability, the diatomite reservoir is developed with 5,060 m^2 (1.25 acre) well spacing. Despite this small well spacing, only 5% of the estimated 2.6 billion barrels of oil in place has been produced since discovery in 1910. In the 1970s, the production of the Lost Hills oil fields was increased by the introduction of hydrofracturing to increase the reservoir permeability. In the 1990s, water floods were added as an EOR technique. In 2000, Chevron USA decided to start a CO_2 pilot project to study the

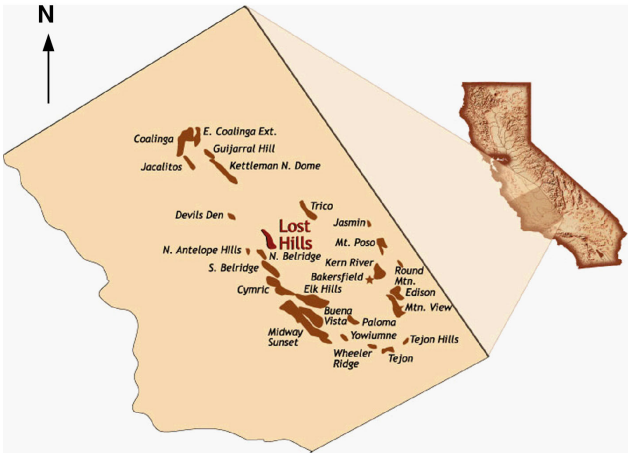

applicability of this technique to the diatomatous reservoir. Initial test were successful resulting in the recovery of 56-65% of the original oil in place (Perri et al., 2000). Despite this success, the location and migration of the CO_2 was unknown, and thus it was decided to use seismic borehole methods to investigate whether the presence and the location of the CO_2 can be estimated.

Previous studies in carbonate reservoirs have shown that CO_2 injection causes seismic velocity changes, which can be mapped spatially using cross well seismic surveys (Wang et al., 1998).

Figure 1: Map indicating the location of the Lost Hills and nearby oil fields in the San Joaquin basin (from Chevron, USA).

The seismic velocity changes can be up to 10%, which is easily detectable and mappable with modern cross well seismic surveys. Therefore, borehole seismic surveys hold promise for mapping and long term monitoring of sequestered CO_2.

Our goal was to investigate, through field testing, the suitability of cross well and single well seismic techniques for imaging subsurface CO_2 and for monitoring geologic sequestration on a finer scale than can be achieved with seismic surface methods. In particular, it was intended to determine whether time-lapse effects can be detected by either method, and whether they are suited to detect a cross-cutting fault and the gas-filled hydrofracture.

Seismic Data Acquisition

The CO_2 injection project at Lost Hills is being operated by Chevron USA. The CO_2 injection began in August 2000 at a relatively low flow rate of 3.5 million m^3 per day. The rate has been gradually increased to the current rate of 12.0 million m^3 per day per injection well. The injection pressure is held at 5.5-6.2 MPa, while the reservoir temperature is about 41 ^oC. The target depth lies between 425 m and 640 m. The effect on seismic velocities and bulk density caused by the presence of CO_2 varies with pressure and temperature. In particular, the transition from liquid phase to gas phase has a dramatic effect on seismic properties as shown by Wang et al. (1998). This is a key point at the Lost Hills site where the injection pressure and temperature are such that a subsurface gas phase of CO_2 is expected. If such gas phase is present, the seismic visibility and mappability should be enhanced. Previous cross well and single well seismic studies have shown the ability to detect a gas-bearing fracture (Majer et al., 1997).

Pre-injection Survey:

The first set of seismic borehole experiments was conducted in August 2000, before the end of the water flood. During this experiment a suite of cross well and single well data sets were acquired using two observation wells 25 m apart. The first survey used a high-frequency (800 - 3500 Hz) piezo-electric P-wave source and hydrophone sensors, while the second survey used an intermediate-frequency (70 - 350 Hz) orbital-vibrator source, generating S-waves that were recorded with 3-component geophones. The third survey was a single well experiment (i.e., source and receivers were placed in the same well) using the piezo-electric source and hydrophone sensors.

The cross well surveys generated P- and S-waves with wavelengths of 1 m and 2.5 m, respectively, providing comparable spatial resolution in both data sets. Figure 2 shows a common receiver gather for the piezo-electric source (a) and the orbital source (b). Although the P-wave data reveal ringing after the onset of the first arrival, the good signal-to-noise-ratio allowed for an accurate determination of the arrival times. The S-wave data is limited in aperture by the presence of Mach-waves that arrive at earlier times on the seismograms for large angle offsets. The presence of these waves limited the use of S-wave arrival times to raypaths that form angles of 45^{o} or less with the horizontal.

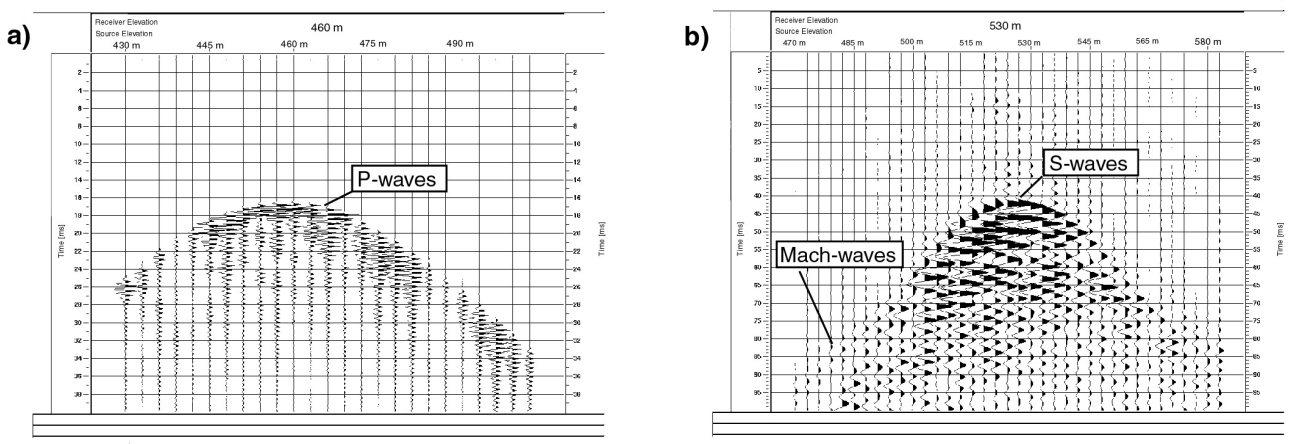

Figure 2: a) Common receiver gather at a depth of 460 m for the pre-injection cross well experiment with the piezo-electric source. **b)** Common receiver gather at a depth of 530 m for the pre-injection cross well experiment with the orbital-vibrator source

Post- CO_2-Injection Survey:

The second set of seismic borehole experiments was conducted in May 2001, after a period of eight months of CO_2 injection. During this experiment a second suite of cross well and single well data sets were acquired using the same source combination as in the pre-injection experiment. However, technical changes in the interim lead to the use of hydrophones as receivers throughout the post-injection survey.

The post-injection cross well data are shown in Figure 3. The P-wave data generated with the piezo-electric source are presented in Figure 3a. It can be seen that the signal-to-noise ratio is comparable to the pre-injection data, and that the resonating character of the data is less pronounced. We attribute this observation to the use of a new hydrophone string in the receiver well. The S-wave data generated with the orbital-vibrator source are shown in Figure 3b. Similar to the pre-injection experiment, both S-wave and Mach-waves can be seen in the common receiver gather.

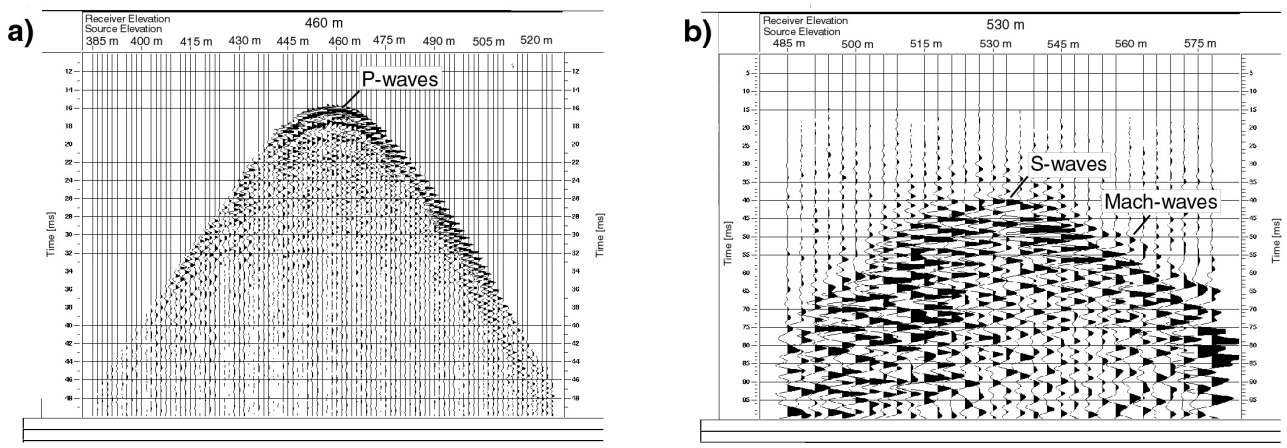

Figure 3: a) Common receiver gather at a depth of 460 m for the post-injection cross well experiment with the piezo-electric source. **b)** Common receiver gather at a depth of 530 m for the post-injection cross well experiment with the orbital-vibrator source.

Cross Well Results

P-wave Data:

In order to determine velocity estimates of the reservoir, the first arrival times for P- and S-waves were determined from the data. The travel time data was inverted using a straight ray back-projection algorithm (Peterson et al., 1985). The inversion process included static time-shifts for each source and receiver location, to account for possible local anomalies around the borehole in the vicinity of sources and receivers, which could map into the velocity estimates if not corrected for.

The P-wave velocity estimates are shown in Figure 4. The results are presented within the reservoir interval from 420 m and 640 m. The location of the sources and receivers are denoted by stars and inverted triangles within the boreholes OB-C1 and OB-C2, respectively. The geologic layering is represented by black lines, while the red line indicates the location of an interpreted fault. Figure 4 represents the velocity estimates for the pre-injection experiment. It can be seen that the velocity varies slightly throughout the reservoir and increases with depth. An apparent transition from slower to higher velocities (1750-1850 m/s) can be seen at about 530 m depth, which is manifested by a change in lithology (Perri et al., 2000). Figure 4b shows the velocity estimates of the post-

injection experiment. It can be seen that the overall velocity dropped about 50-80 m/s throughout the reservoir. The main velocity structure is similar to that of the pre-injection test with no apparent localized change in the pattern that could indicate the location of CO_2. To better analyze the subtle temporal changes between the pre- and post-injection data, we compute the differences (pre-minus-post) between the two velocity tomograms. The results are displayed in Figure 4c. It can be seen

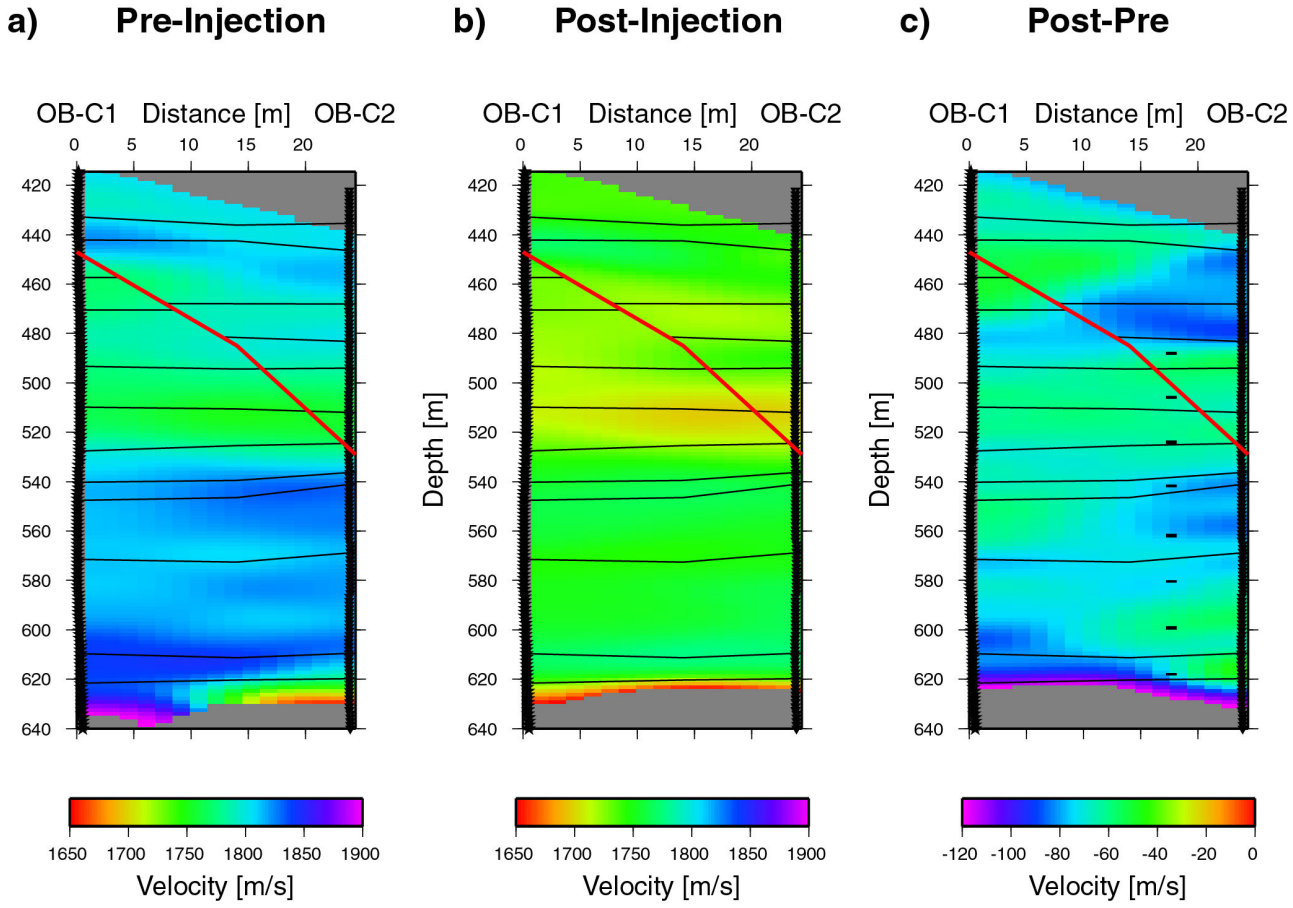

Figure 4: P-wave velocity estimates based on travel time data. **a)** Pre-injection estimates. **b)** Post-injection estimates. **c)** Result of differencing the Pre-Post injection estimates. The black dashes represent the projection of the CO_2 injection intervals onto the imaging plane.

that the maximum velocity decrease is about 90 m/s (~5%) visible above the injection interval between 440-480 m depth, at intermediate depth from 540-560 m, and in the lower part of the reservoir at 600 m depth. The top anomaly appears to be located between well OB-C2 and the fault, which seems to be partly inhibiting the extension of the anomaly towards well OB-C1. If this is a manifestation of the presence of CO_2, the gas must have migrated upwards above the fractured interval, caused by a possible extension of the fracture to shallower depth.

S-wave Data:

The pre-injection S-wave velocity estimates (Figure 5a) corroborate the results of the P-wave data. The transition from upper to lower reservoir diatomite is clearly visible at about 530 m depth. Although the inversion resulted in very low S-wave velocity estimates between 550-850 m/s, these values are not uncommon for this soft reservoir rock (Bourbie et al., 1987). The S-wave velocity structure is similar to that of the P-waves with a low velocity layer between 440-480 m, followed

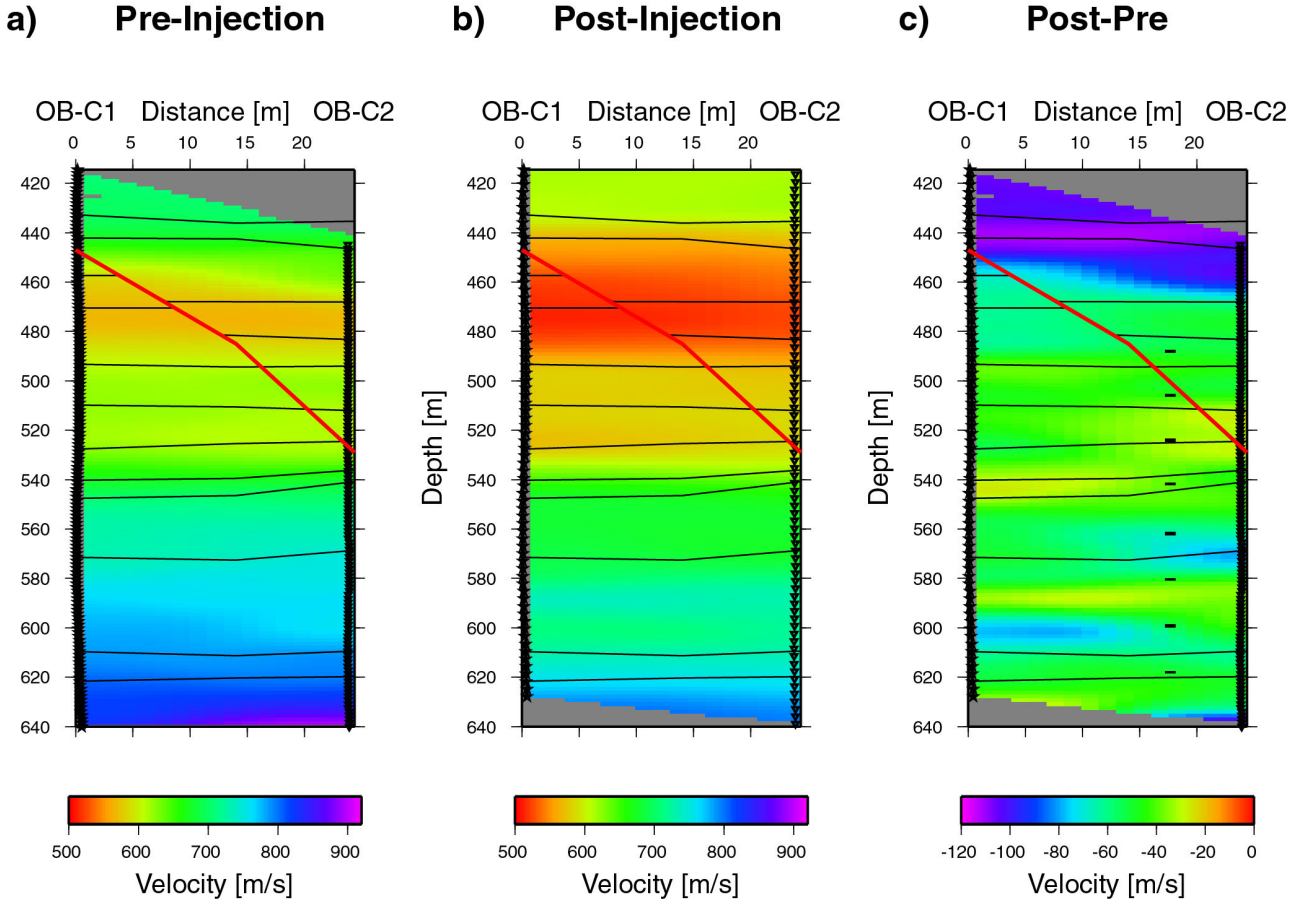

Figure 5: S-wave velocity estimates based on travel time data. **a)** Pre-injection estimates. **b)** Post-injection estimates. **c)** Result of differencing the Pre-Post injection estimates. The black dashes represent the projection of the CO_2 injection intervals onto the imaging plane.

by intermediate velocities between 500-520 m depth, and a sharp transition to lower reservoir properties at 530 m depth. However, the spatial resolution of the S-wave data is limited by the predominantly sub-horizontal ray coverage. The post-injection results in Figure 5b reveal a velocity drop of about 50-80 m/s while the overall structure of the velocity image remains the same. Again, no apparent location of CO_2 is visible. The differenced results in Figure 5c reveal a maximum decrease of 75 m/s (~9%) (the anomaly across the top of the image of -120 m/s is less reliable because of the limited ray coverage along the top of the reservoir, which was different for the pre- and post S-wave surveys). In comparison to the maximum P-wave velocity difference at 440-480 m between well OB-C2 and the fault, the S-wave velocities reveal an intermediate decrease of 60 m/s

for the same location. However, in the central and bottom part of the reservoir (560-580 m and 600 m depth) the S-wave velocity reveals decreased values comparable to those of the P-wave velocity.

The time-lapse velocity estimates for P- and S-waves show good correlation throughout the reservoir, although they represent independent data sets as they were excited by different seismic sources. At this point, however, the common interpretation does not yield a unique answer about the state of CO_2 in the reservoir. If CO_2 is present in gas form and the pore pressure does not change (i.e., gas displaces pore fluid), the P-wave velocity would decrease while the S-wave velocity would remain constant, as the S-wave is not sensitive to changes in gas or fluid saturation. However, since the S-wave velocities decrease, a pressure increase is likely to have occurred during the CO_2 injection phase. In this case, both P- and S-wave velocities would decrease since the differential pressure (confining-minus-pore pressure) would decrease. This scenario is possible for the case of free gas as well as for the case of the dissolution of CO_2 into the liquid phase in the reservoir. To answer the question of the state of the CO_2 of the reservoir, we calculate the Poisson ratio and interpret the results in the next section.

Poisson Ratio:

The Poisson ratio (PR) is calculated based on the velocity estimates for P- and S-waves shown in Figures 4 and 5 as

$$\nu = \frac{0.5\left(V_P/V_S\right)^2 - 1}{\left(V_P/V_S\right)^2 - 1} \qquad (1)$$

Figure 6a shows the PR for the pre-injection experiment. The estimates mimic the trend of the P- and S-wave velocity estimates, which is not necessarily expected, because the velocity effects could cancel in Equation 1. The PR shows a clear separation into the upper and lower reservoir diatomite with the transition at 530 m depth, as shown before. The high PR in the upper reservoir section is caused by the low S-wave velocity estimates, however, PR of 0.42-0.45 are not uncommon for this highly porous rock (Bourbie et al., 1987). The decrease in PR with depth indicates the compaction of the diatoms accompanied by a decrease in density (Bilodeau, 1995).

The post-injection estimates (Figure 6b) are similar to the pre-injection values, with the exception of higher values in the upper reservoir (440-460 m), where the S-waves velocities were particularly low.

The difference in PR is shown in Figure 6c. It can be seen that the time-lapse changes resulted in an increase in PR throughout the reservoir (the negative values at the bottom are an artifact of the inversion process caused by limited ray coverage). These results support the preliminary findings derived from the velocity inversions. If a free gas is present and the pore-pressure increases (which is necessary in our case to explain the drop in S-wave velocity) the PR would decrease as shown by Dvorkin et al. (1999) and Mallick (2001). However, if the gas is in solution (i.e., the medium is fluid saturated) and the pore-pressure increases, the PR increases as reported by Detournay and Cheng (1993), Dvorkin et al. (1999), and Simpson (2001). In a similar study Dvorkin and Nur (1996) support this conclusion by showing that for water saturated high porosity sandstone (20-40%) the PR increases with decreasing confining pressure. To evaluate the estimates for the PR as

shown in Figure 6c, we calculate the change in PR using a rock properties model (Gassmann, 1951). The result is an increase in PR with an average value of 0.0045. In comparison, the average value of the increase in PR in Figure 6c is 0.0074 +/- 0.0052 yielding estimates in line with the prediction of the rock properties model (Hoversten et al., 2003).

Thus a possible conclusion that can be drawn from the interpretation of the PR is that CO_2 has dissolved into the liquid phase in the reservoir rock and increased the pore pressure in several

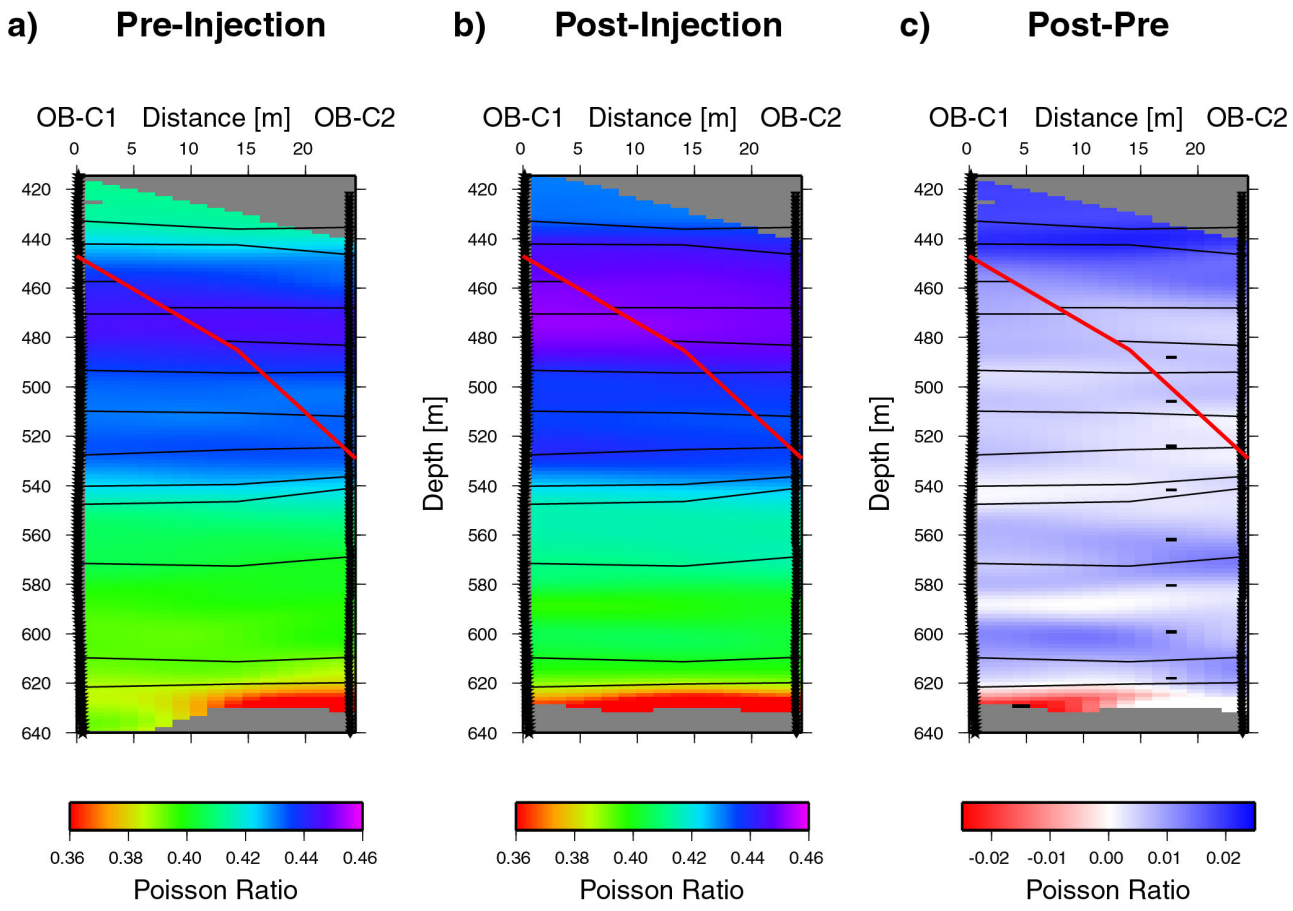

Figure 6: Poisson ratio based on the P- and S-wave velocity estimates in Figures 4 and 5. **a)** Pre-injection ratio. **b)** Post-injection ratio. **c)** Result of differencing the Pre-Post injection ratios. The black dashes represent the projection of the CO_2 injection intervals onto the imaging plane.

compartments inside the reservoir. Figure 6c suggest that CO_2 migrated horizontally in the lower section of the reservoir around 570 and 600 m depth. The strong increase at the top of the reservoir above 440 m is likely an artifact resulting from low resolution of the S-wave estimates. However, the slight increase visible above the top of the injection interval may indicate an over-pressurization of the reservoir caused by an upward migration of the CO_2, as the PR should have remained constant otherwise. However, it is also possible that some of the regions that reveal an increase in PR have undergone a pore-pressure increase caused by the injection process without the CO_2 actually reaching these zones.

In the following, the results of the cross well experiment will be compared to the single well data.

Single Well Results

A conceptual model of a single well seismic experiment is shown in Figure 7, where a source emits seismic energy, which propagates to receivers below (a reverse geometry where the source is located below the receivers has also been used for single well imaging in the past). The direct waves reach farther into the medium compared to sonic logging because the source-receiver offset and the wavelengths of the waves are longer. At the same time, waves propagate outwards from the well and reflect off interfaces above and below and off features like faults and fractures that may be present in the medium.

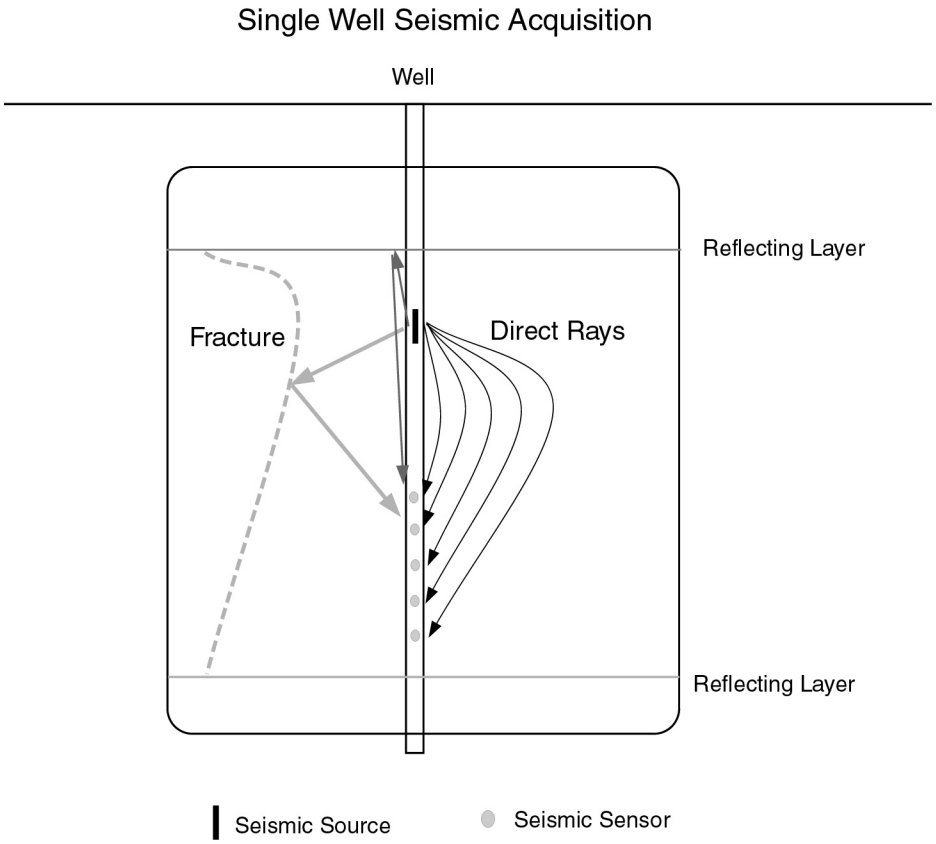

Figure 7: Wave propagation in single well seismic data acquisition. The sketch displays the principle of wave propagation from the source to the receivers along direct or reflected ray paths.

The direct arrival times of the P-waves (pre- and post-injection) and the S-waves (post-injection) were determined from the single well data collected in well OB-C1. The results are plotted in Figure 8. The pre-injection results are shown in Figure 8a. The thick gray line represents the velocity measurements from the single well data, while the thin black line is an average velocity combining the estimates of the three pixels adjacent to the source well OB-C1 at each depth position (horizontal average over 5m). Although static source corrections have been accounted for, the average yields a better comparison because the P-waves of the single well data propagate farther out from the well. The different depth ranges are the result of different acquisition intervals caused by different receiver strings and source-receiver offsets. The fit is good, nevertheless, indicating that the near borehole effects (i.e., borehole cement, borehole anulus) present in many sonic log velocity data, play only a minor role in the present case as the longer wavelengths integrate the effects farther away from the borehole. This result corroborates the velocity estimates

of the travel time inversion. The post-injection P-wave results are presented in Figure 8b. The dashed line represents results of ultrasonic velocity measurements by Chevron, USA, on cores taken 126 m west of the CO_2 injection site. The overall fit between the single- and cross well

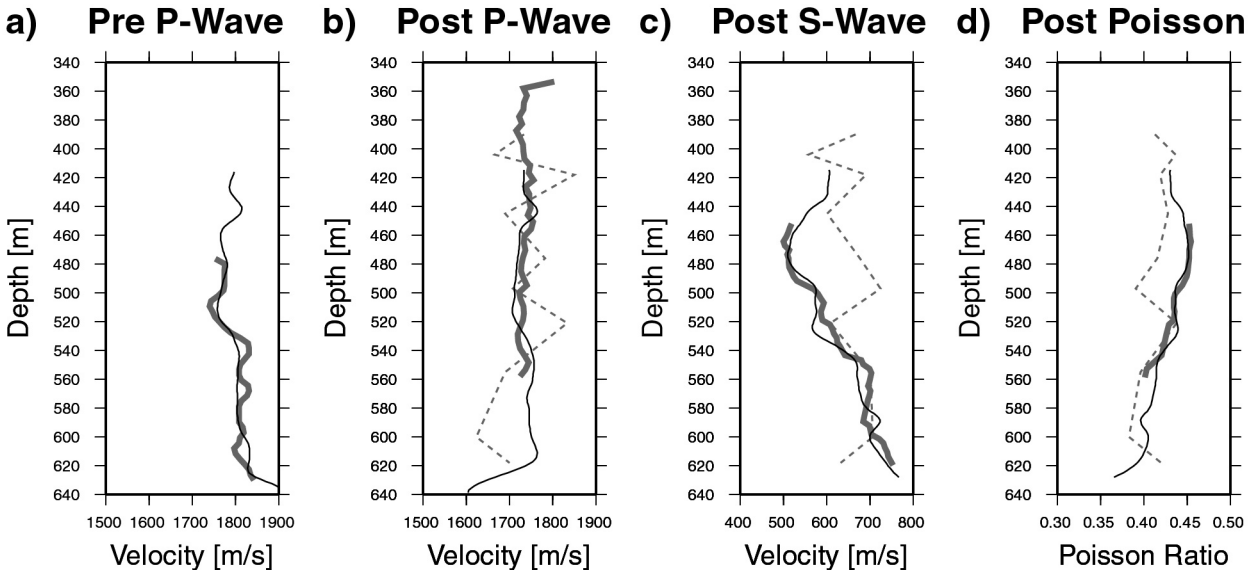

Figure 8: Comparison between cross well and single well estimates of the velocities and the Poisson ratio. The thin line represents a 5 m horizontal average of estimates along the source borehole from tomographic studies, while the thick line represents the results of the single well study. The dashed line represents the results of ultrasonic measurements on cores retrieved in the vicinity of the CO_2 injection site. **a)** Pre-injection P-wave estimates. **b)** Post-injection P-wave estimates. **c)** Post-injection S-wave estimates. **d)** Post-injection Poisson ratio.

results is good, although the single well data did not cover the lowermost section of the reservoir. Although the ultrasonic P-wave velocity measurements reveal more variation throughout the depth range, the average values fall within the range of the field measurements. The comparison of the cross- and single well S-wave field data in Figure 8c reveals a good fit even down to details in the velocity structure (i.e., velocity increase with depth, velocity inversion between 460-480 m depth). The ultrasonic results show higher values in the upper reservoir, while they match the field data in the lower reservoir section. Finally, the post-injection PR is plotted in Figure 8d. The result of the single well experiment is limited to the depth range where post P- and S-wave data overlap. However, even for this limited depth range the fit between the two graphs representing the field data is very good, revealing an overall decrease of the PR with increasing reservoir depth. The lower values at the bottom of the reservoir are in accordance with the transition from diatomite to a more shaley rock, which exhibits PR between 0.35-0.40. The PR of the core data was computed based on equation (1) using the ultrasonic velocities as shown in Figure 8a and b. As expected from the trend of the S-wave data, the fit is better in the lower half of the reservoir.

In summary, the results of the single well data independently confirm the results of the cross well experiment. Therefore, when available, both experiments should be run simultaneously to determine the reliability of the velocity estimates.

Conclusions

The goal of the current experiment was to investigate whether the location and migration of CO_2 or its effects in geologic sequestration processes can be imaged with seismic borehole methods. The time-lapse borehole experiment was conducted over a period of one year, during which a series of cross- and single well experiments resulted in the successful acquisition of P- and S-wave data.

The separate results of the cross well experiments showed no clear indication of the location of the fault between the two observation holes. However, differencing the P-wave velocity estimates revealed the possible location in form of an abrupt termination of a velocity anomaly. At the same time there was no evidence of the hydrofracture in the cross well results.

The P-wave and S-wave velocity estimates showed a decrease in value over the course of the CO_2 injection phase, indicating a possible increase in pore pressure throughout the reservoir. However, using the velocity estimates alone, it was not possible to determine whether the CO_2 exists in gas from or whether it dissolved into the liquid phase of the reservoir. After the Poisson ratio was calculated from the velocities, however, it was concluded that the CO_2 had dissolved into the liquid phase, as the time-lapse results revealed an increase in PR. This shows the advantage of simultaneous acquisition of P- and S-wave data. The tomographic images suggested the extension of the hydrofracture to a shallower section of the reservoir above the intended fracture interval.

The concurrent acquisition of single well data enabled us to verify the results of the cross well survey. The wavelengths excited in the single well experiment are long enough to sample the medium in the vicinity of the well without too much interference from borehole effects as in the case of sonic logging. Therefore, the velocity estimates are more representative of the medium, and, as in our case, could be used to independently verify the results of the cross well survey. Both experiments can be readily conducted at the same time and offer the possibility to verify common results, while they provide complementary information that adds to the general understanding of the reservoir properties.

Acknowledgements

The authors like to acknowledge Michael Morea and Chevron USA Production for their generous help with field information, and the release of the ultrasonic core data. This work was supported by the GEO-SEQ project of the DOE National Energy Technology Laboratory (NETL) under contract no DE-AC03-76SF000098. Support was also provided by Chevron USA Production Co. and the National Petroleum Office under Contract No. DE-FC22-95BC14938, Class III Field Demonstration Project. Data processing was carried out at Berkeley Lab's Center for Computational Seismology, while field work and data collection were supported by Berkeley Lab's Geophysical Measurement Center. Both centers are supported by the Director, Office of Science, Office of Basic Energy Sciences, Division of Engineering and Geosciences, of the U.S. Department of Energy under Contract No. DE-AC03-76SF00098.

References

Bilodeau, B.J., 1995, Determining Water Saturation in Diatomite using Wireline Logs, Lost Hills Field, California, Proceedings SPE/AAPG Western Regional Meeting, SPE 29653, pp. 369-382.

Bourbie, T., Coussy, O., Zinszner, B., 1987, Acoustics of Porous Media, Gulf Publishing Company, Houston, 1987, pp. 334.

Detournay, E., Cheng, H., 1993, A short course on poroelasticity in rock mechanics: constitutive equations - theoretical background, Proc. U.S. Rock Mech. Symp., 34th, pp. 1-28.

Dvorkin, J., and Nur, A., 1996, Elasticity of high-porous sandstones: Theory for two North Sea data sets, Geophysics, Vol. 61, No. 5, pp. 1363-1370.

Dvorkin, J., Mavko, G., Nur, A., 1999, Overpressure detection from compressional- and shear-wave data, Geophys. Res. Lett., Vol. 26, No. 22, pp. 3417-3420.

Gassmann, F., 1951, Elasticity of porous media: Ueber die Elastizitaet poroeser Medien, Vierteljahrschrift der Naturforschenden Gesellschaft, Vol. 96, pp.1-23.

Hoversten, G.M., Gritto, R., Washbourne, J., Daley, T.M., 2003, CO_2 Gas/Oil Ratio Prediction in a Multi-Component Reservoir by Combined Seismic and Electromagnetic Imaging, Geophysics, in press.

Mallick, S., 2001, AVO and elastic impedance, The Leading Edge, Vol.20, No.10, pp. 1094-1104.

Majer, E.L., Peterson, J.E., Daley, T.M., Kaelin, B., Queen, J., D'Onfro, P., and Rizer. W, 1997, Fracture detection using cross well and single well surveys, Geophysics, Vol. 62, No. 2, pp. 495-504.

Perri, P.A., Emanuele, M.A., Fong, W.S., and Morea, M.F., 2000, Lost Hills CO_2 pilot: evaluation, design, injectivity test results and implementation, Proceedings SPE/AAPG Western Regional Meeting, SPE 62526, pp. 13.

Peterson, J.E., Paulson, B.N., and McEvilly T.V., 1985, Applications of algebraic reconstruction techniques to cross hole seismic data, Geophysics, Vol. 50, No. 10,pp. 1566-1580.

Simpson, G., 2001, Influence of compression-induced fluid pressures on rock strength in the brittle crust, J. Geophys. Res., Vol. 106, No. B9, pp. 19,465-19,478.

Wang, Z., Cates, M.E., and Langan, R.T., 1998, Seismic monitoring of a CO_2 flood in a carbonate reservoir: A rock physics study, Geophysics, Vol. 63, No. 5, pp. 1604-1617.